Journal of Solid State Chemistry 181 (2008) 3116–3120

Contents lists available at ScienceDirect

Journal of Solid State Chemistry

journal homepage: www.elsevier.com/locate/jssc

Large-scale growth of millimeter-long single-crystalline ZnS nanobelts

Jianye Li [a,*], Qi Zhang [b], Lei An [a], Luchang Qin [b], Jie Liu [a,*]

[a] Department of Chemistry, Duke University, Durham, NC 27708, USA
[b] Department of Physics and Astronomy, University of North Carolina at Chapel Hill, Chapel Hill, NC 27599, USA

ARTICLE INFO

Article history:
Received 4 May 2008
Received in revised form
27 July 2008
Accepted 4 August 2008
Available online 17 August 2008

Keywords:
Nanocrystalline materials
ZnS

ABSTRACT

Millimeter-long single-crystalline hexagonal ZnS nanobelts were grown on specific locations on a wafer scale. This is the first time that the millimeter-scale ZnS nanobelt has been synthesized. The longest nanobelts are about 3 mm. The as-grown nanobelts were characterized by means of field emission scanning electron microscopy, X-ray powder diffraction, high-resolution transmission electron microscopy, and selected area electron diffraction. The results indicate that the ultra-long nanobelts are pure single-crystalline hexagonal ZnS. There are two kinds of ZnS nanobelts existing in the products. One is the nanobelts that have two smooth sides and grow along the [0 0 1] longitudinal direction, and the other is the nanobelts that have one smooth side and one saw-teeth-like side, namely nanosaws, and grow along the [2 1 0] longitudinal direction. A vapor–liquid–solid mechanism is suggested for the lengthwise growth of the ZnS nanobelts (nanosaws) and a vapor–solid mechanism for the side direction growth of the saw-teeth of the nanosaws.

1. Introduction

Hexagonal zinc sulfide (ZnS), an important II–VI group semiconductor with a direct wide bandgap of 3.7 eV at room temperature, has been extensively studied due to its wide applications as excellent phosphors, photocatalysts, and so on [1–5]. As an important luminescence material, ZnS shows various luminescence properties such as photoluminescence, electroluminescence, mechanoluminescence, acousticluminescence, thermal luminescence, and triboluminescence [2,5]. ZnS also exhibits optical transparency in a wide range, from the visible light (0.4 μm) to the deep infrared region (12 μm). In addition, attributed to its large exciton binding energy (40 meV) and small Bohr radius (2.4 nm), ZnS is an excellent candidate in exploring the intrinsic recombination processes in dense excitonic system [1–8]. It has been widely used in the fields of ultraviolet light-emitting diodes, injection lasers, flat-panel displays, cathodes-ray tube luminescence, thin film electroluminescent devices, infrared (IR) windows, sensors, solar cells, and so forth [1–8].

Nanocrystalline ZnS has been reported to have some characteristics different from the bulk crystal, which may extend its applications [2,9]. Recently, a great deal of attention has been focused on the study of one-dimensional ZnS materials for their broad prospects in fundamental physical science research, novel nanotechnological applications, and significant potential for optoelectronics [1–8,10–16].

Nanobelt (or nanoribbon) is a unique one-dimensional nanostructure with a rectangular cross-section and the semiconductor nanobelts (or nanoribbons) were first reported in 2000 [17]. In the past few years, ZnS nanobelts have attracted considerable attention for their significant potential applications [1,2,5–8,11–16]. So far, ZnS nanobelts have been designed as oxygen sensors [14], hydrogen sensors [16], and field emitters [15] for prospective applications.

In this report, we demonstrated that through a simple vapor-phase transport process, single-crystalline hexagonal ZnS nanobelts with a length up to 3 mm were location-controlled grown on a large scale for the first time. Millimeter-long nanobelts are very important for the highly efficient preparation of nanobelt devices. It is effortless to fabricate many nanodevices with a millimeter-long nanobelt and it can greatly guarantee the identity of the devices. We believe this simple approach for wafer-scale preparation of the millimeter-long single-crystalline ZnS nanobelts will greatly facilitate the large-scale industrial applications of ZnS nanobelts.

There are two kinds of ZnS nanobelts in the products synthesized using this method: one is the nanobelts that have two smooth sides and grow along the [0 0 1] longitudinal direction, and the other is the nanobelts that have one smooth side and one saw-teeth side (nanosaws), and grow along the [2 1 0] longitudinal direction. We have found out that the length of the saw-teeth of the ZnS nanosaws increases proportionally with the distance between the substrate, where we collect the products in

* Corresponding authors.
E-mail addresses: jianye-li@northwestern.edu (J. Li), jliu@chem.duke.edu (J. Liu).

0022-4596/$ - see front matter © 2008 Elsevier Inc. All rights reserved.
doi:10.1016/j.jssc.2008.08.009

the growth system, and source materials while the length of the ZnS nanosaws decreases proportionally with the distance. When the distance is larger than 11 cm, the saw-teeth-like ZnS nanostructures evolve to comb-like ZnS nanostructures (namely nanocombs). The growth mechanisms of the ZnS nanobelts and nanosaws are discussed. The longitudinal direction of the ZnS nanobelts (nanosaws) grows through a vapor–liquid–solid (VLS) mechanism, and the side direction of the saw-teeth of the nanosaws via a vapor–solid mechanism.

2. Experimental section

The setup we used to grow the ZnS nanobelts is similar to that designed to prepare GaN nanowires, described in a previously published paper [18]. The growth was carried out in a horizontal fused quartz tube mounted on a tube furnace, and a mixture of ZnS (99.99%, Alfa Aesar) and graphite carbon (99.9995%, Alfa Aesar) powders with a ratio of 2:1 was used as the source material. The substrates used to deposit the ZnS nanobelts are Au film (30 nm thick) patterned on n-type silicon wafers with 1 μm thermal oxide (Silicon Quest). The Au patterns were generated by the standard photolithography and thermal evaporation [19]. Separated by a distance of 5–10 cm, the source material and the gold-patterned substrates were loaded into an alumina boat, and the boat was placed at the center of the horizontal quartz tube. After the quartz tube was purged with a flow of argon (99.99%, National Specialty Gases.) of about 2000 standard cubic centimeters per minute (sccm) for 2 h, the furnace was heated under a steady flow of argon of about 100–300 sccm to 900 °C. The temperature was kept constant at 900 °C for 5–8 h. Then the furnace was switched off and allowed to cool down to room temperature. Large pieces of yellowish, wool-like products were formed on the substrates. Finally, the products were characterized by field emission scanning electron microscopy (FESEM, Philips FEI XL30SFEG), X-ray powder diffraction (XRD, Rigaku Multiflex X-ray diffractometer with Cu $K\alpha$ radiation at room temperature), and transmission electron microscopy (TEM, JEM 2010F).

3. Results and discussion

XRD measurements were performed on bulk samples to assess the overall crystal structure and phase purity of the products. Fig. 1 is a typical XRD pattern of the prepared product and it can be indexed to a hexagonal wurtzite structure of ZnS. These data match well with the reported standard values of hexagonal ZnS with lattice constants of $a = 0.3822$ nm and $c = 0.6260$ nm (Joint Committee on Powder Diffraction Standards (JCPDS) Card no. 36–1450). The XRD result reveals that the nanobelt products have a pure hexagonal ZnS phase. The relatively strong (002) peak suggests that the ZnS nanobelts are partially aligned.

Fig. 2a is a representative low-magnification FESEM image of the ZnS nanobelts and it shows that the millimeter-long ZnS nanobelts were obtained on a large scale. FESEM image also reveals that the ultra-long ZnS nanobelts were grown on the catalyst-patterned substrates with the longest nanobelts of 3 mm. (see Fig. S1). Figs. 2b and c are the high-magnification FESEM images of the millimeter-long nanobelts, and it can be seen that the thickness of the nanobelts is within several tens of nanometers and the width ranges from several hundred nanometers to about 3 μm.

Fig. 3a shows the lattice-resolved high-resolution TEM (HRTEM) image of a ZnS nanobelt and it clearly reveals the (001) atomic planes with an inter-planar spacing of 0.63 nm along the lengthwise direction of the nanobelts and the (100) atomic

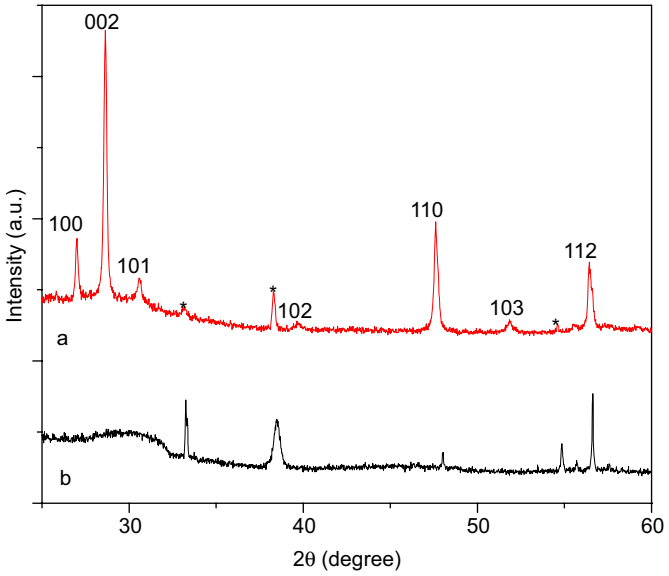

Fig. 1. Room temperature XRD patterns measured using Cu $K\alpha$ radiation. (a) The millimeter-scale ZnS nanobelts grown on a Au-patterned substrate (the peaks with * in the XRD pattern are from the substrates), and (b) a Au-patterned substrate without the growth of the ZnS nanobelts.

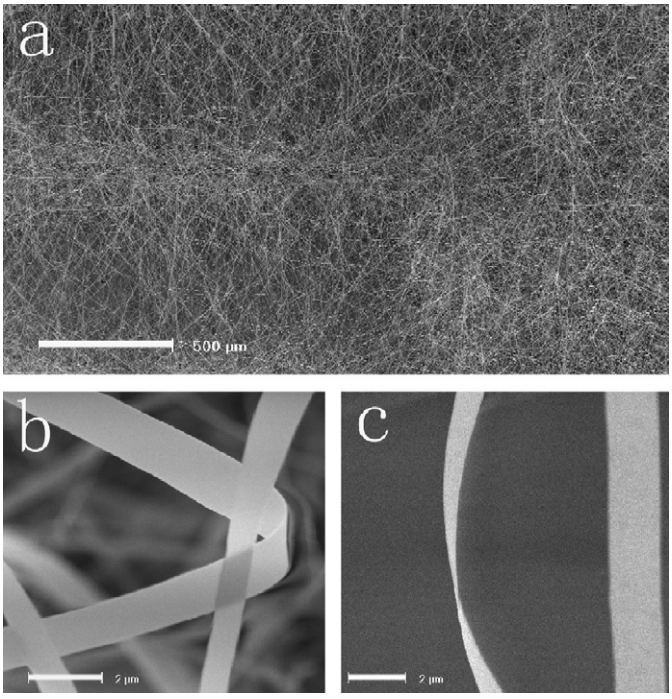

Fig. 2. (a) Low-magnification FESEM image of the ZnS millimeter-long nanobelts. The scale bar is 500 μm. (b and c) High-magnification FESEM images of the ZnS nanobelts, and the thickness of the nanobelts is less than 60 nm. Both the scale bars are 2 μm.

planes with an inter-planar spacing of 0.33 nm along the widthwise direction of the nanobelts. The longitudinal and widthwise directions of the ZnS nanobelt are [0 0 1] and [2 1 0], respectively. The selected area electron diffraction (SAED) pattern of an individual ZnS nanobelt has been studied to further assess the structure of the nanobelts (Fig. 3b). The SAED pattern can be indexed as a hexagonal structure with lattice constants of $a = 0.38$ nm and $c = 0.63$ nm recorded along the [0 1 0] zone axis, which is consistent with the above XRD and HRTEM results. The

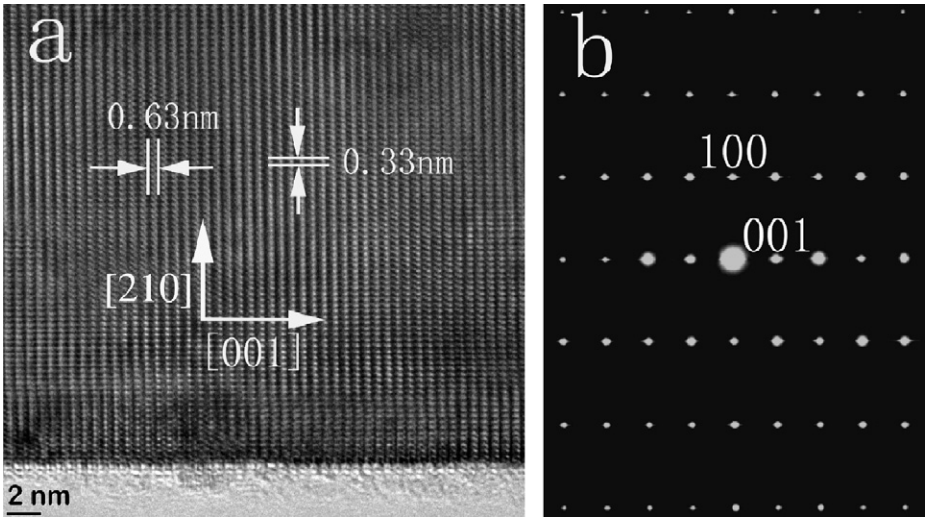

Fig. 3. (a) HRTEM image of a section of a ZnS nanobelt. The scale bar is 2 nm. (b) SAED pattern of a ZnS nanobelt recorded along the [010] zone axis.

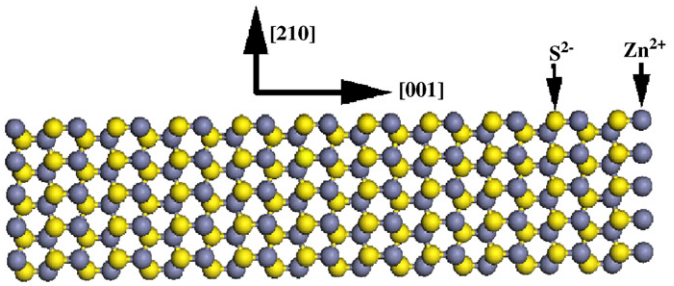

Fig. 4. A structure model of the ZnS nanobelt and the nanobelt grows along the [0 0 1] direction.

perfect SAED pattern and lattice fringes indicate that the ZnS nanobelts are structurally uniform and single-crystalline hexagonal structures. As confirmed by the HRTEM image and the SAED pattern, the millimeter-long ZnS nanobelts generally grow along the [0 0 1] direction. A structure model of the ZnS nanobelts was constructed as in Fig. 4, and [0 0 1] and [2 1 0] are the longitudinal and widthwise directions of the nanobelts, respectively.

In addition to the millimeter-long ZnS nanobelts with two smooth sides, ultra-long hexagonal ZnS nanobelts with one saw-teeth-shaped side and one smooth side were also found in the product. Fig. 5 is the FESEM image of the saw-like ZnS nanobelts (ZnS nanosaws). The thickness of most of the ZnS nanosaws is within several tens of nanometers and the width from several hundred nanometers to several microns.

To ascertain their structure, the ZnS nanosaws were further characterized by TEM. Fig. 6a is low-magnification TEM image of a ZnS nanosaw and the one-sided teeth morphology is clearly seen. Figs. 6b and c are the lattice-resolved HRTEM images taken from two areas of the ZnS nanosaw and they reveal the single-crystalline hexagonal structure of the ZnS nanosaws. Fig. 6b is an HRTEM image from a section of the nanosaw close to the smooth side and it shows the (100) atomic planes with an inter-planar spacing of 0.33 nm along the lengthwise direction of the nanosaw and (001) atomic planes with an inter-planar spacing of 0.63 nm along the widthwise direction of the nanosaw. In other words, the longitudinal and widthwise directions of the ZnS nanosaws are [2 1 0] and [0 0 1], respectively. Fig. 6c is an HRTEM image of a saw-tooth of the ZnS nanosaw and it indicates the saw-teeth grown along the [0 0 1] direction, parallel to the widthwise

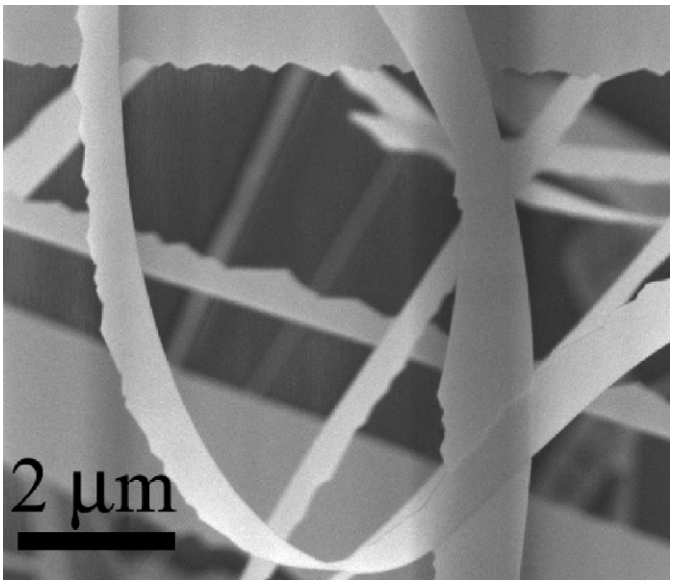

Fig. 5. FESEM image of the saw-like ZnS nanobelts (ZnS nanosaws) and the one-sided tooth structure is clearly seen.

direction of the nanosaw and perpendicular to the [2 1 0] growth direction of the nanosaw.

An interesting result was observed from the HRTEM analysis. When growing along the [0 0 1] direction, [0 0 1] and [2 1 0] are the longitudinal and widthwise directions, respectively, and the two smooth-sided ZnS nanobelts were formed. When growing along the [2 1 0] direction, the ZnS nanosaws were produced. Contrary to the directions of the ZnS nanobelts, the longitudinal and widthwise directions of the ZnS nanosaws are [2 1 0] and [0 0 1], respectively.

VLS mechanism is common for the formation of one-dimensional semiconductor nanomaterials and it is evident that the ultra-long ZnS nanobelts reported here grow via a VLS mechanism [20,21]. Two typical evidences suggest a VLS growth of the millimeter-long ZnS nanobelts: (1) the ZnS nanobelts only grow on the surfaces with gold-patterned catalysts; (2) the catalyst particles at the ends of the nanobelts can be observed, and EDX analysis indicates only the particles contain element gold (see Fig. S2). A proposed growth model for the ZnS nanobelts is

shown in Fig. 7. At 900 °C, with the assistance of graphite carbon (graphite carbon was used to lower the growth temperature by decreasing the vaporizing temperature of the ZnS [22]), ZnS powders those located at the center of furnace vaporized. Through the flow of argon, the vapor-phase ZnS is transported downstream to the lower temperature zone where the substrates located. The substrates zone has a temperature of 840–880 °C, and at this temperature, the patterned gold films formed liquid gold drops on the substrates. To test this hypothesis, we annealed the gold-patterned substrate and the substrate located downstream at a distance of 7 cm from the furnace center. After annealing with the central temperature of 900 °C under a steady flow of argon of 250 sccm for 5 h, gold particles formed on the surface of the substrate (see Fig. S3). As energetically favored sites for absorption of vapor-phase ZnS, the hot liquid gold droplets on the substrates absorbed the vapor-phase ZnS and when the ZnS reached saturation, ZnS nanobelts began to nucleate and grow. With the continuous steady absorption, nucleation and growth, wafer-scale millimeter-long ZnS nanobelts were grown on the substrate. The key for the growth of millimeter-long nanobelts is keeping a steady and continuous growth during the total growth process. Otherwise, no millimeter-long ZnS nanobelts obtained.

Same as the long ZnS nanobelts, the long ZnS nanosaws were only grown on the gold-patterned substrates and catalyst particles at the ends of the nanosaws were also observed. These evidences suggest that the longitudinal direction growth of the nanosaws is also a VLS mechanism. On the other hand, the side direction growth (saw-teeth direction growth) of the ZnS nanosaws could be a vapor–solid (VS) mechanism [23] because no catalyst particles were detected on the tops of the saw-teeth. As the nanobelts grow along the lengthwise direction, the ZnS vapor is also downstream transported to the sides of the ZnS nanobelts that are being grown. In this lower temperature zone, the supersaturated ZnS vapor solidified and ZnS saw-teeth formed via a VS process. Wang et al. [24] suggested that the polar surfaces caused the saw-teeth structure of hexagonal wurtzite crystal structure. For wurtzite ZnS crystal structure, the Zn-terminated (0 0 1) surface is chemically active, while the S-terminated (0 0 $\bar{1}$) surface is relatively inactive [25]. The difference in surface activities brings about the VS growth of the one-sided saw-teeth along the [0 0 1] direction.

The ZnS nanosaw-teeth's length increased with the distance between the substrate and the source material while the length of

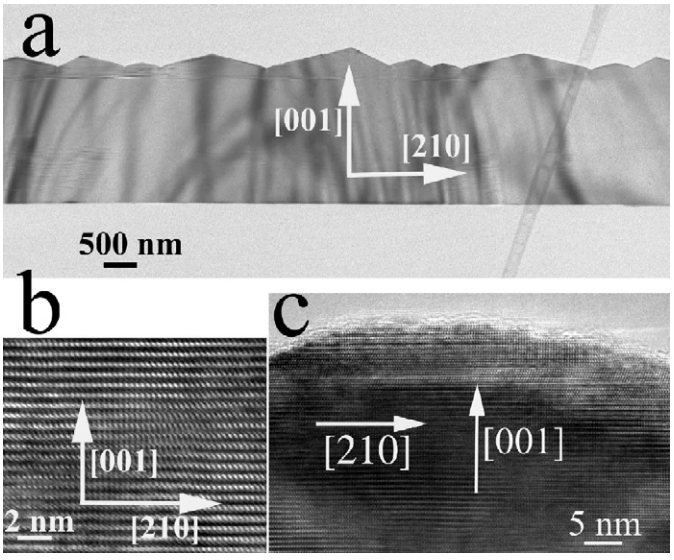

Fig. 6. (a) Low-magnification TEM image of a ZnS nanosaw. (b) HRTEM image of a section close to the smooth side of the ZnS nanosaw. (c) HRTEM image of a saw-tooth of the ZnS nanosaw.

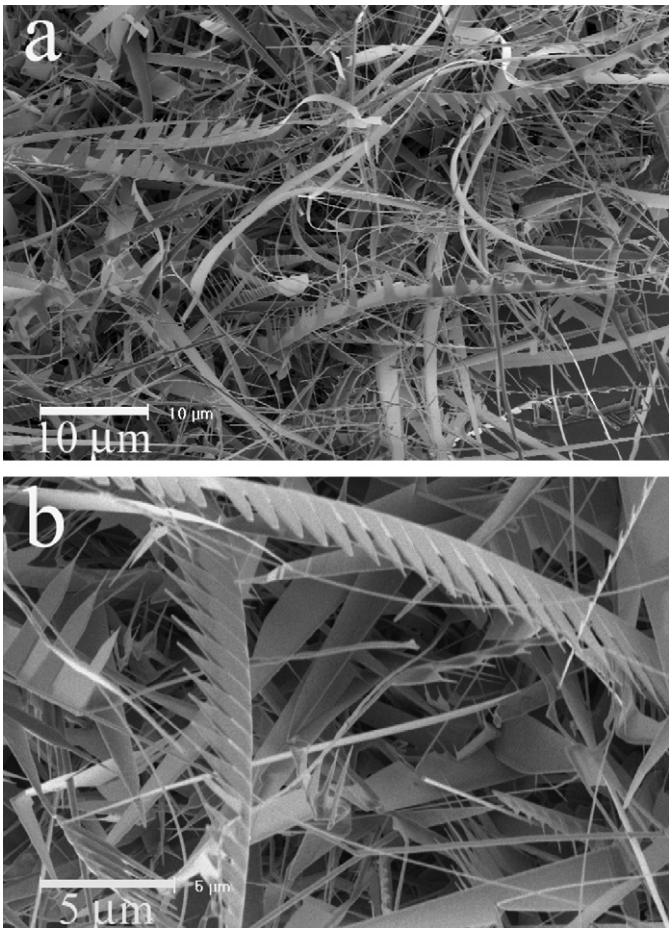

Fig. 8. FESEM images of the ZnS nanoscombs.

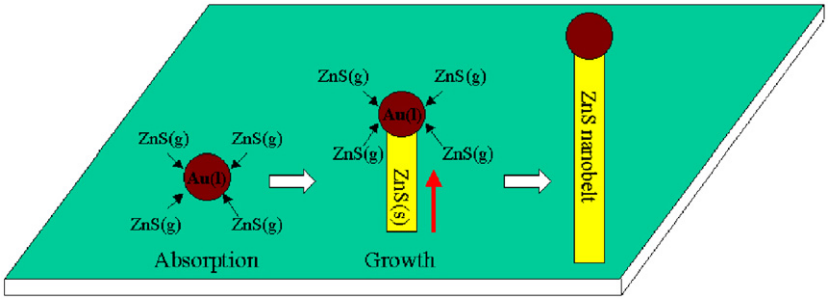

Fig. 7. Proposed growth model of the ZnS nanobelt.

the ZnS nanosaws decreased with the distance. The larger the distance, the lower the substrate zone's temperature is. With a lower temperature, the performance of the liquid gold drops to serve as energetically favored sites to absorb vapor ZnS weakens, and the longitudinal VLS growth slows down. At the same time, the solidifying speed of ZnS vapor increases and the side VS growth speeds up. When the distance is larger than 11 cm, the ZnS saw-teeth nanostructures evolve to comb-like nanostructures, namely nanocombs (see Fig. 8). It is found that the length of the comb-teeth is not identical and shortens symmetrically as the comb-teeth became close to the catalyst tips at the ends of the nanocombs. This is a result of the competition between the two different growths, the VLS longitudinal growth and the VS side growth of the nanocombs. The comb-teeth that close to the catalyst tip form later and have shorter length.

4. Conclusions

In summary, millimeter-long hexagonal ZnS nanobelts were location-controlled grown on a wafer-scale for the first time. The XRD, HRTEM, and SAED results indicate the ultra-long nanobelts are pure hexagonal ZnS single crystals. The length of the longest nanobelts is about 3 mm. There are two kinds of ultra-long ZnS nanobelts existing in the products. The nanobelts with two smooth sides grow along the [0 0 1] longitudinal direction, and the saw-like nanobelts with one smooth side and one saw-tooth-like side grow along the [2 1 0] longitudinal direction. The length of the saw-tooth of the ZnS nanosaws increases proportionally with the distance between the substrate and the source material while the length of the ZnS nanosaws decreases with the distance. A VLS mechanism was suggested for the longitudinal direction growth of the ZnS nanobelts (nanosaws) and a VS mechanism for the side direction growth of the saw-teeth of the nanosaws. This simple approach for wafer-scale growth of millimeter-long single-crystalline ZnS nanobelts will open up many opportunities for further fundamental studies and greatly facilitate the large-scale industrial applications of ZnS nanobelts.

Appendix: Supporting information available

FESEM image of the ZnS nanobelts with a length up to 3 mm, FESEM image of a ZnS nanobelt with a catalyst particle at its end and the EDX spectrum of the catalyst particle, and FESEM image of the annealed gold-patterned substrate.

Acknowledgments

This work is supported in part by Grant no. 49620-02-1-0188 from Air Force Office of Scientific Research (AFOSR).

Appendix A. Supplementary materials

Supplementary data associated with this article can be found in the online version at doi:10.1016/j.jssc.2008.08.009.

References

[1] C. Ma, D. Moore, J. Li, Z.L. Wang, Adv. Mater. 15 (2003) 228.
[2] Y. Jiang, X.M. Meng, J. Liu, Z.Y. Xie, C.S. Lee, S.T. Lee, Adv. Mater. 15 (2003) 323.
[3] Y. Jiang, X.M. Meng, J. Liu, Z.R. Hong, C.S. Lee, S.T. Lee, Adv. Mater. 15 (2003) 1195.
[4] Q. Li, C.R. Wang, Appl. Phys. Lett. 82 (2003) 1398.
[5] Y. Zhu, Y. Bando, D.F. Xue, Appl. Phys. Lett. 82 (2003) 1769.
[6] Q. Li, C.R. Wang, Appl. Phys. Lett. 83 (2003) 359.
[7] Y. Zhu, Y. Bando, D.F. Xue, D. Golberg, Adv. Mater. 16 (2004) 831.
[8] B.Y. Geng, L.D. Zhang, G.Z. Wang, T. Xie, Y.G. Zhang, G.W. Meng, Appl. Phys. Lett. 84 (2004) 2157.
[9] N.A. Dhas, A. Zaban, A. Gedankan, Chem. Mater. 11 (1999) 806.
[10] C.J. Barrelet, Y. Wu, D.C. Bell, C.M. Lieber, J. Am. Chem. Soc. 125 (2003) 11498.
[11] X.M. Meng, Y. Jiang, J. Liu, C.S. Lee, I. Bello, S.T. Lee, Appl. Phys. Lett. 83 (2003) 2244.
[12] P.A. Hu, Y.Q. Liu, L. Fu, L.C. Cao, D.B. Zhu, Issue Series Title: J. Phys. Chem. B108 (2004) 936.
[13] Y. Hao, G. Meng, Z.L. Wang, C.H. Ye, L.D. Zhang, Nano Lett. 6 (2006) 1650.
[14] Y.G. Liu, P. Feng, X.Y. Xue, S.L. Shi, X.Q. Fu, C. Wang, Y.G. Wang, T.H. Wang, Appl. Phys. Lett. 90 (2007) 042109.
[15] X. Fang, Y. Bando, G. Shen, C. Ye, U. Gautam, P.M. Costa, C. Zhi, C. Tang, D. Golberg, Adv. Mater. 19 (2007) 2593.
[16] Z. Chen, J. Zou, G. Liu, H.F. Lu, F. Li, G.Q. Lu, H.M. Cheng, Nanotechnology 9 (2008) 055710.
[17] J.Y. Li, Z.Y. Qiao, X.L. Chen, Y.G. Cao, Y.C. Lan, C.Y. Wang, Appl. Phys. A17 (2000) 587.
[18] J.Y. Li, C.G. Lu, B. Maynor, S.M. Huang, J. Liu, Chem. Mater. 16 (2004) 1633.
[19] B.W. Maynor, J.Y. Li, C.G. Lu, J. Liu, J. Am. Chem. Soc. 126 (2004) 6409.
[20] A.M. Morales, C.M. Lieber, Science 279 (1998) 208.
[21] X.F. Duan, C.M. Lieber, J. Am. Chem. Soc. 122 (2000) 188.
[22] X. Wang, C.J. Summers, Nano Lett. 4 (2004) 423.
[23] J.Y. Li, X.L. Chen, Solid State Commun. 131 (2004) 769.
[24] Z.L. Wang, X.Y. Kong, J.M. Zuo, Phys. Rev. Lett. 91 (2003) 185502.
[25] D. Moore, C. Ronning, C. Ma, Z.L. Wang, Chem. Phys. Lett. 385 (2004) 8.